RSC Advances

ROYAL SOCIETY OF CHEMISTRY

www.rsc.org/advances

Synthesis and characterization of new hydrodesulphurization Co-Mo catalysts supported on calcined and pyrolyzed bone

M. Emami Yazdani[a], B.H. Monjezi[a], M. Mokfi[a], H. Bozorgzadeh[b], A. Gil[c] and M. Ghiaci[a,*]

[a]Department of Chemistry, Isfahan University of Technology, P.O. Box. 84156-83111, Isfahan, Iran

[b]Gas Research Center, Research Institute of Petroleum Industry, Tehran, Iran

[c]Department of Applied Chemistry, Public University of Navarra, 31006 Pamplona, Spain

Corresponding author: Tel.: +98 311 3913254; fax: +98 311 3912350

E-mail address: mghiaci@cc.iut.ac.ir

Abstract:

A series of cobalt-molybdenum catalysts supported on calcined bones (hydroxyapatite, HAP) and pyrolyzed bones (hydroxyapatite-carbon, HAP-C) have been prepared by impregnation method. The catalysts were characterized by XRD, FT-IR spectroscopy, UV-Vis spectroscopy, TPR, TPD of CO_2, BET, FE-SEM, EDX and TEM techniques. Hydrodesulphurization (HDS) experiments were carried out in a fixed-bed reactor at 15 bar hydrogen pressure, liquid hourly space velocity (LHSV) 4.5 1/h, the volumetric hydrogen/feed ratio of 175 NL/L and 310 ^{o}C. HDS reactions of dibenzothiophene (DBT), dimethyl disulfide (DMDS) and industrial naphtha over synthesized catalysts were investigated. The Co-Mo/HAP-C and Co-Mo/HAP catalysts displayed a satisfactory performance comparable with the commercial catalyst. Co-Mo/Al_2O_3 and Co-Mo/HAP catalysts were tested for hydrodesulphurization of DMDS, and Co-Mo/HAP showed a higher activity than the commercial catalyst (Co-Mo/Al_2O_3) and lowered the sulfur content of the feedstock from 2500 ppm to 9 ppm.

Keywords: Hydrodesulphurization; calcined bone; pyrolyzed bone; Naphtha; Co-Mo nano-catalyst

1. Introduction

The exhaust gases from vehicles are a major source of air pollution through the production of NO_x and SO_x, and because of the environmental regulations the amount of sulfur permitted in fuels and gas oil is limited to <0.01 wt.%. Moreover, sulfur is a poison for catalytic converters [1]. Therefore, reduction of sulfur content of crude oil, light gas oil, and oil-derived feedstock for the petrochemical industries using catalytic HDS is a routine operation in petroleum refining processes [2-4]. In this process the feedstock mixture passes over a catalyst which breaks the sulfur-carbon bonds, allowing the sulfur to react with hydrogen to form hydrogen sulfide. There are a number of hydrodesulphurization catalysts, that the most commonly used catalysts consist of sulfides of transition metals especially molybdenum sulfide, and also contain cobalt as promoter [5,6].

Since cobalt or nickel promoted molybdenum-tungsten sulfides are well established as the active species for commercial HDS, a major goal of this research focuses on the use of new types of supports for developing high performance HDS catalysts. Different supports have been used for designing new hydrotreating catalysts. The nature of the support has an important role in activity of the catalysts. The most commonly used support is alumina because of its excellent mechanical and dispersion properties [7]. Interesting data have been published in regard to improving the HDS catalyst performance, including the use of new supports like MgO [8], ZrO_2 [9,10], TiO_2 [11,12], carbon [13-15], zeolites like Na–Y [16,17], mesoporous materials like MCM-41 [18] and HMS [19,20] as catalyst support. The present work examines the potential of two new materials as supports for the Co-Mo catalyst in the hydrodesulphurization reaction that are made of bone source, calcined bones (HAP) and pyrolyzed bones (HAP-C).

HAP (Ca_{10} $(PO_4)_6(OH)$ $_2$), is a natural calcium phosphate, and major constituent of human bone and teeth. Bone inorganic composition (bone mineral) is formed from carbonated hydroxyapatite with lower crystallinity. The structure of the Ca–P solid phase in bone was first identified by Dejong in 1926 as a crystalline calcium phosphate similar to geological apatite by chemical analysis and most importantly by X-ray diffraction [21]. Structure of pure hydroxyapatite is very similar to that of bone but there are tiny differences between them due to the presence of other ions such as iron in the structure of bone hydroxyapatite.

What was the idea behind this work? We know that bone is a porous firm organic matrix that is invigorated with calcium and phosphate salts. If we expose bone to a solution containing a specific metal ion, one would expect that because of the capillary properties of the bone it could adsorb metal ions to a limited amount into its matrix, and when the bone is calcined, we will end up with well-dispersed metal oxides over the hydroxyapetite. In this regard, we tried to prepare a series of new catalysts which contain oxides of different metals in nanosize. In our previous works [22,23], we demonstrated the application of nanoparticles of manganese and cobalt oxides in oxidation of 2,6-diisopropylnaphthalene, diphenylmethane, and anthracene. In exploring this idea, we tried to immobilize the oxides of cobalt and molybdenum in nanosize on hydroxyapatite and use them in hydrodesulphurization reaction. Therefore, we decided to prepare the catalyst in three different ways: (1) by osmosis; (2) by impregnation on calcined bone (hereafter this support is called HAP), and (3) on pyrolyzed bone (hereafter this support is called HAP-C); in this way, we expected that the carbon of the organic materials in bone remains and would disperse on the HAP. The prepared Co-Mo catalysts were tested in the hydrodesulphurization process of three different samples, ie. industrial naphtha, dimethyl disulfide and dibenzothiophene.

One of the feeds i.e., naphtha is a complex mixture of paraffins, naphthenes and aromatics in the C_5 to C_{12} range. Naphtha from catalytic or thermal cracking also contains olefins. Naphthas of different origins contain small amounts of additional compounds containing elements such as sulfur and nitrogen. These elements affect the performance of the bifunctional noble metal catalyst used in catalytic reforming and must be removed to low levels with hydrodesulphurization reaction prior to entering the reformer unit [24]. DBT is among the molecules present in the fuel which is very difficult to desulphurize and causes problems in deep HDS [25]. However, DMDS is easily desulphurized because of its linear and unstrained structure.

The present paper examines the potential of calcined bone HAP and HAP-C as new supports for Co-Mo catalysts in hydrodesulphurization of DBT, DMDS and industrial naphtha. Such model compounds represent the most refractory sulfur compounds found in petroleum products. The catalysts prepared were investigated in terms of their activity and selectivity and the results were compared with those of a conventional Co-Mo/Al_2O_3 commercial catalyst.

2. Experimental

2.1. Synthesis of the supports

In this study, bone was used as a source of the hydroxyapatite. Pieces of cow bone were cleaned, dried at 100 ºC. Then, the bones were burned for 8 h on the flame until a black powder was obtained. At the end of process, black powder was calcined at 700 ºC for 2 days and HAP was obtained as a white powder.

For synthesis of the HAP-C, bones were pyrolyzed in the N_2 atmosphere. Temperature range of pyrolysis was 100-700 ºC with intervals of 50 ºC and kept the temperature constant for 2 h in each step. At the end of pyrolysis program, a black powder was obtained that was called HAP-C.

2.2. Synthesis of the catalysts

2.2.1. Preparation of the bone supported catalyst by osmosis method

In the first step, 0.493 g (1.69 mmol) $Co(NO_3)_2 \cdot 6H_2O$ and 0.919 g (0.74 mmol) ammonium heptamolybdate tetrahydrate ($(NH_4)_6Mo_7O_{24}.4H_2O$, Merck) were dissolved in 500 mL of deionized water so that the molar ratio of Co/Mo was 0.33 in the resultant solution. The reason for choosing this ratio was that we wanted to load the support with 2 wt.% cobalt and 10 wt.% molybdenum because the commercial hydrodesulphurization catalysts almost contain 2 and 10 wt.% cobalt and molybdenum, respectively. Pieces of cow bone were cleaned, piecemealed and were put into the resultant solution for a period of one week. After one week, the pieces of the bone were extracted from the solution. We expected that cobalt and manganese were loaded on the support. Attained sample was dried at 100 °C, and finally calcined/pyrolyzed at 700 °C for 24 h to obtain Co/Mo-BSO and Co/Mo-BSO-C. The cobalt and molybdenum contents of the synthesized catalyst samples i.e., Co/Mo-BSO and Co/Mo-BSO-C were determined by ICP-AES. The molar ratio of the measured Co and Mo contents in the supported catalysts was 1.8, and 1.84 respectively; this means that the diffusion of cobalt into the bone framework has happened more efficiently than molybdenum. As mentioned before, the commercial hydrodesulphurization catalysts usually contain 2 and 10 wt.% cobalt and molybdenum, respectively and one would not expect to observe a reasonable activity for these catalysts.

2.2.2. Preparation of the bone supported catalyst by impregnation method

For preparation of this catalyst, an aqueous solution containing 0.78 g of cobalt nitrate hexahydrate ($Co(NO_3)_2.6H_2O$, Merck), and 1.45 g of ammonium heptamolybdate tetrahydrate ($(NH_4)_6Mo_7O_{24}.4H_2O$, Merck) was prepared, and then 7 g of the support (HAP or HAP-C) was added into the solution. The mixture was dried at room temperature, and then calcined under nitrogen protection at 450 °C in a closed container. The catalyst contains Co and Mo in 2 and 10 wt %, respectively.

2.3. Characterization

FT-IR spectra were recorded in the range of 4000–400 cm^{-1} using 100 scans with a JASCO FT-IR (680 plus) using pellets with spectroscopic grade potassium bromide (KBr). Diffuse reflectance spectra were recorded in the range of 250- 600 nm with a JASCO UV-Vis 550. X-ray diffraction (XRD) patterns of the catalysts were measured using Philips X pert model MPD analytical diffractometer using Cu Kα radiation (λ = 1.54 A˚). The operating condition of XRD was at 40 kV and 30 mA in step scan mode. The scans were recorded in the 2θ range between 10-80º. Nitrogen adsorption isotherms were measured by the conventional static volumetric method using a Micromeritics Digisorb 2600 instrument. Transmission electron microscopy (TEM) was carried out on the powder samples with a Tecnai F30 TEM operating at an accelerating voltage of 300 kV. A high-resolution Hitachi S4160 field emission scanning electron microscope outfitted with an EDX system (FE-SEM/EDX) was used for the scanning electron microscopy measurements. The TPR/TPD experiments were conducted in a semiautomatic Micromeritics TPD/TPR 2900 apparatus.

2.4. Catalytic activity for hydrodesulphurization

All of the catalysts were tested in a fixed-bed reactor. A stainless steel temperature controlled tube with an inner diameter of 20.6 mm was used as the reactor. The reactor was placed in an electric furnace capable of heating up to 800 °C. The temperature of the furnace was adjusted by a JUMO, ITRON 08 Temperature Indicator Controller (TIC). In this device two thermocouples were used. One was used to control the temperature of the furnace, and the second one was connected to the reactor at the center of the catalyst bed. All temperature measurements reported in this study refer to the temperature measured by the reactor thermocouple. A high-pressure syringe pump (ISCO Model 260D) was used to pump the liquid feedstock into the reactor. Hydrogen flow rate was measured and controlled using a Brook's mass flowmeter. A back-pressure regulator was used to control the system pressure.

Also the gas flow rate was controlled by a Brook's 0154 MFC read out which was calibrated for different flow rates of hydrogen. The reaction products were conducted into a condenser continuously where they were cooled down. The condensed liquid phase was used for total sulfur measurement.

For each run, 7 g of the catalyst was diluted with silicon carbide. The top and bottom of the catalyst bed was packed with silicon carbide as the diluents. Before the hydrodesulphurization reaction, the catalyst was sulfided in situ with a mixture of 1 wt.% dimethyl disulfide in ISOMAX (jet fuel). Sulfidation reaction was performed under 30 bar hydrogen pressure, LHSV of mixture 2.5 1/h and hydrogen to sulfidation mixture ratio of 175 NL/L. The sulfidation temperature changed with a defined program. The temperature was increased from room temperature up to 180 °C with heating rate of 40 °C/h, then with heating rate of 20 °C/h from 180 to 260 °C. After this step, the sulfidation product was injected into the reactor, and the temperature was increased at a rate of 10 °C/h from 260 to 310 °C, finally kept at this temperature for 12 h until the sulfidation reaction became complete. After sulfidation reaction, the feed was changed to HDS feed and reaction was performed at 310 ºC , LHSV of 4.5 1/h, the volumetric hydrogen/feed ratio of 175 NL/L and hydrogen pressure was decreased to 15 bar which well approximated industrial conditions. The reaction took place for a definite time (20-72 h). After the HDS reaction, products were collected through a condenser and the final sample was used for total sulfur analysis. The total sulfur content of the feed and products were analyzed by using an ASTM D5453 analyzer. The Co-Mo/HAP-C catalyst was tested with three model hydrocarbon feeds (1) industrial naphtha containing 2890 ppm of sulfur, (2) naphtha containing sulfur less than 1 ppm that used as a solvent and dimethyl disulfide as a source of sulfur; the concentration of sulfur in this mixture was 2510 ppm, (3) the naphtha that was used in the third feed contains dibenzothiophene as a source of sulfur; concentration of sulfur in this mixture was 3370 ppm. The Co-Mo/HAP catalyst and the commercial catalyst (Co-Mo/Al_2O_3) were tested with the second model feed stock.

3. Results and discussion

3.1. Characterization of the catalysts

3.1.1. FT-IR spectroscopy

The IR spectra of the catalysts are shown in Fig. 1. The IR spectrum of the HAP-C support shows absorption bands in the range of 1300-1700 cm^{-1} that were attributed to the

presence of the carbon in the structure of HAP-C. The absorption band at 1040 cm^{-1} in the IR spectra of the supports and the catalysts arises from $\upsilon_3PO_4^{3-}$, and the bands at 603 and 561 cm^{-1} arise from $\upsilon_4PO_4^{3-}$. When the metals (Co and Mo) were immobilized on the supports a new broad band in the range of 750-850 cm^{-1} was appeared that was assigned to the vibrations of the Mo–O–Mo bridging bonds in both catalysts. In the Co-Mo/HAP-C catalyst the absorption band at 960 cm^{-1} also was assigned to the vibrations of the Mo–O–Mo bridging bonds and another absorption band at 478 cm^{-1} was assigned to vibration of Co-O bond [7]. In the Co-Mo/HAP catalyst the absorption band of Co-O bond was overlapped with the absorption bands of the HAP support.

3.1.2. UV-Vis spectroscopy

DR-UV–Vis spectroscopy provides information about the different oxidation states and local coordination geometry of supported Co and Mo oxides species. It should also be mentioned that the calcined cow bone has some trace transition metal elements [22] that might affect on the UV-Vis DRS spectra of the catalysts. The results are shown in Fig. 2. The changes and appearance of new absorption bands in the electronic spectra of the prepared catalysts could reflect the coordination of Co and Mo. It is known [26,27] that Mo tetrahedral species absorb at 250 to 280 nm, while Mo in octahedral coordination state present transitions at 230 to 330 nm. The DRS experiments indicate that most of the Mo species in Co-Mo/HAP and Co-Mo/HAP-C catalysts are in the octahedral state, and the absorption bands are characteristic of polymeric Mo-O-Mo structures which exhibit charge transfer from O^{-2} to Mo^{+6} with an octahedral coordination. The transition due to octahedral Mo species in Co-Mo/HAP shifts its position significantly with respect to the Co-Mo/HAP-C.

The broad band around 400-500 nm confirms the presence of both tetrahedral and octahedral Co species. The band could be assigned to the surface cobalt species formed during calcination with tetrahedral and octahedral cobalts [26].

3.1.3. X-ray diffraction

Fig. 3 shows the XRD patterns of the calcined CoMo/HAP and CoMo/HAP-C catalysts, and the diffraction pattern of HAP is marked for comparison. The diffraction patterns of HAP with the characteristic peaks located at around 24.5, 28, 36.1, 44.1, 46.5, 56.2, 74.8º could be distinguished in all samples. For the CoMo/HAP catalyst, there are peaks attributable to molybdenum oxide which is formed on the surface of the support. In contrast,

the CoMo/HAP-C presents diffraction peaks of $CoMoO_x$ with the characteristic peaks located at around 28, 32, 33, 39, 42, and 47 as shown in Fig. 3(b). The possible reason for formation of $CoMoO_x$ on the surface of HAP-C might be because of hydrophobic nature of this support.

3.1.4. Texture of the catalysts

The data are evaluated by the standard BET, t-Plot and Langmuir methods. Nitrogen adsorption isotherms of the catalysts are shown in Fig. 4. The catalysts isotherms are similar to isotherm of type II in the IUPAC categorization which is typical for macroporous materials. At low relative pressure monolayer adsorption of adsorbed molecules occurs, while at high relative pressure a multilayer adsorption takes place. In the case of adsorption where capillary condensation occurs, hysteresis loops appear. These hysteresis loops have been classified in a way similar to the IUPAC adsorption isotherm. These isotherms have hysteresis loops like type H3 that conventional interpretation of these hysteresis loops is slit-like pores for which adsorbent–adsorbate pair would yield a type II isotherm without pores [28].

From the slope of the t-Plot isotherms and related equations some information about texture of the catalysts was obtained that are summarized in Table 1. Results of BET and Langmuir equation are also shown in Table 1. BET measurements displayed a low surface area (4.18 m^2/g) for the Co-Mo/HAP catalyst; even by having a low surface area, the activity of this catalyst was very well in HDS process of DMDS. Result of BET analysis for the Co-Mo/HAP-C catalyst discovered a higher surface area of 101.70 m^2/g.

3.1.5. TEM

More information about the catalysts morphology and size distribution could be deduced from TEM characterizations. Fig. 5 shows the TEM images of the catalysts. From these images one could deduce that the size of nanoparticles is in the range of 20-60 nm. From data of textural properties of the two catalysts it is clear that one would expect to have a more dispersed cobalt and molybdenum species in the Co-Mo/HAP-C catalyst. Moreover, the presence of carbon in this catalyst could play some role in deposition of the metals on the surface of the support (HAP-C). As a general conclusion from the TEM images, we could say that the metal species in the Co-Mo/HAP-C are more dispersed than in the Co-Mo/HAP. It is also clear that the metal species in the Co-Mo/HAP-C catalyst are smaller than the metal species in the Co-Mo/HAP catalyst. Moreover, the size of nanoparticles of MoS_2, and MoS_2

containing Co might affect on the shape of the nanoparticles that according to the Wulff construction determines which edges will be exposed, and these parameters might show themselves in catalytic activity of the catalysts.

3.1.6. FE-SEM-EDX

The FE-SEM images were carried out to determine the morphology of the two catalysts. The FE-SEM images show that Co-Mo/HAP-C catalyst has a more porous structure than Co-Mo/HAP. Particles size was determined to be 18.8 nm for Co-Mo/HAP catalyst and 22-29 nm for Co-Mo/HAP-C catalyst. For obtaining evidence for the uniform deposition of active phase in the catalysts, and utilization of elemental composition, the energy-dispersive analysis of X-ray (EDAX) was used, and results are shown in Fig. 6. The quantitative analysis of different elements has shown that 1.68 wt.% Co and 11.58 wt % Mo exist in the Co-Mo/HAP catalyst and 1.48 wt.% Co and 10.15 Mo wt.% are present in the Co-Mo/HAP-C catalyst.

3.1.7. Temperature-Programmed Reduction (TPR)

TPR experiments give profitable information about the degree of interaction of the metals with the supports. Fig. 7(b) shows the TPR profiles of the CoMo/HAP and CoMo/HAP-C catalysts, and TPR profiles of HAP, Co/HAP, Mo/HAP are included for comparison, Fig. 7(a). The reduction of CoMo catalysts supported on HAP and HAP-C occurs in the temperature range of 350-900 ºC. Both catalysts have three hydrogen uptake peaks at about 438, 530 and 690 ºC. The $CoMo/Al_2O_3$ also has three main hydrogen consumption peaks which occur approximately at the temperatures (520, 595 and >900 ºC) close to the uptake peaks of these new catalysts. The TPR profiles of the new catalysts show that the reduction is probably completed at 900 ºC due to the reduction of highly dispersed molybdenum oxide species. The high temperature reduction peak might be ascribed to the strong interaction between the small precursor species and the support. Clearly, one might expect that HAP presents a much stronger interaction compared with HAP-C. It is also apparent that the reduction of Co will promote the reduction of molybdenum oxides. Hydrogen can be dissociated on the more easily reduced Co sites at comparatively lower temperatures, and such hydrogen spills to the molybdenum sites and reduction occurs. For Co-Mo/HAP catalyst the peak around 436 ºC is due to the partial reduction of Mo^{6+} to Mo^{4+} (octahedral Mo). The peak at higher temperature (690 ºC) represents the reduction of Mo^{4+} to Mo^0, in other words, tetrahedrally coordinated molybdate group [29]. The reduction of

$CoMoO_4$ takes place in two steps at 518 ºC and 707 ºC [3]. Therefore the peak at 518 ºC could also be assigned to the reduction of this phase. For the Co-Mo/HAP-C catalyst, as shown in Fig. 7b, the peak at around 439 ºC corresponds to reduction of Mo^{6+} to Mo^{4+} (octahedral Mo), and another peak at 686 ºC is related to reduction of tetrahedrally coordinated molybdate group. The broad peak at 546 ºC in Co-Mo/HAP-C may represent the intermediate species between tetrahedral and octahedral Mo species [30]. Also it should be mentioned that the reduction of $CoMoO_4$ takes place at about this temperature. It is clear that the Co-Mo/HAP-C catalyst has completed its reduction at around 760 ºC when the Co-Mo/HAP catalyst has consumed some hydrogen up to 850 ºC. This probably means that in the Co-Mo/HAP catalyst there exist highly dispersed molybdenum oxide species strongly interacting with the support. Despite that Co-Mo/HAP-C catalyst has much more surface area but the presence of carbon in this catalyst has accumulated cobalt and molybdenum species, and $CoMoO_x$ phase was formed on the surface of HAP-C. In other words, the presence of carbon may induce interaction between Co and Mo, and as a result of this interaction $CoMoO_x$ was formed. It is interesting that the amount of hydrogen consumed in the Co-Mo/HAP catalyst is higher than consumed hydrogen in the Co-Mo/HAP-C catalyst. This has shown itself in the higher reactivity of the Co-Mo/HAP catalyst.

3.1.8. Temperature programmed CO_2 desorption (TPD)

The temperature programmed desorption of CO_2 was carried out to demonstrate the total basicity of the synthesized catalysts. Fig. 8 shows the TPD-CO_2 curves of the catalysts before and after reduction. It is clear that the reversible adsorption sites of CO_2 are surface P-OH groups on the HAP particles, and we believe that during adsorption and desorption of CO_2, calcium carbonate could not be formed because of stronger electrostatic forces between Ca^{2+} ions and phosphate ions. As seen in the Fig. 8, the temperatures that peaks have appeared on CO_2 desorption curves are different for each catalyst. If simple desorption of CO_2 molecules occurs during pretreatment, the basic sites should be weak, and the basic sites should be strong if desorption occurs at high temperatures [31,32]. As shown in Fig. 8(a), for the Co-Mo/HAP catalyst desorption of CO_2 takes place at 50 ºC, which means that this catalyst has very weak basic sites. For the Co-Mo/HAP-C catalyst, two peaks appear on 650 ºC and 759 ºC, which show that this catalyst has strong basic sites and also has two different basic sites. We do not really have a reason for different basicity of the two catalysts before reduction. After reduction of the both catalysts, their TPD curves have changed and CO_2

desorption occurred at higher temperature. Therefore, it may be concluded that these catalysts after reduction with H_2 are more basic than before reduction.

3.2. Co-Mo/HAP and Co-Mo/HAP-C catalyst activity in HDS of DMDS

A naphtha containing 2510 ppm sulfur (as DMDS) was selected as model compound for the HDS reaction to evaluate the activity of the novel Co-Mo/HAP and Co-Mo/HAP-C catalysts relative to the commercial catalyst. Both catalysts were tested under identical experimental conditions. Residual sulfur content of the feed after treatment was determined and results are shown in Table 2. As shown in Table 2, Co-Mo/HAP catalyst after 48 h could decrease the sulfur content of the feed to 9 ppm while the commercial catalyst at the same conditions decreased the sulfur content of the same feed to 107 ppm and this catalyst after 72 h could decrease the sulfur content of the feed to 24 ppm. Therefore Co-Mo/HAP catalyst has shown a much higher activity than the commercial catalyst. Co-Mo/HAP-C catalyst was also tested with DMDS feed. From Table 2, one could clearly observe that the Co-Mo/HAP-C catalyst could reduce sulfur content of feed from 2510 ppm to 110 ppm after 20 h while the commercial catalyst reduces the sulfur concentration of feed to 930 ppm after 24 h, so even the Co-Mo/HAP-C catalyst has shown a higher activity than the commercial catalyst. The lower activity of the commercial catalyst in comparison with these catalysts i.e., Co-Mo/HAP and Co-Mo/HAP-C, may be related to the presence of some Mo-O-Al linkages between the MoS_2 and (or) Co-Mo-S and the alumina support. CO_2-TPD measurements have shown that these new catalysts have strong basic sites, and such linkages could not exist. In other words, S-Mo-S and Co–Mo–S without strong linkages with the support could be more active. Lower activity of Co-Mo/HAP-C in comparison with Co-Mo/HAP might be related to the size of the metal nano-clusters. As a matter of fact, HDS occurs by means of parallel hydrogenation (HYD) and direct desulfurization (DS) routes; turnover rates for both routes decreased with decreasing metal species size because the stronger sulfur binding at the surfaces of small species decreases the concentration of the required sulfur vacancies during steady-state HDS catalysis. The sulfur binding strength at the metal surfaces also depends strongly on metal identity [33].

3.3. Feed effect in the HDS reaction

Ability of a catalyst to remove sulfur from a feed depends on feed composition. Therefore the catalytic performance of the sulfided Co-Mo/HAP-C nano-catalyst in terms of conversion was examined in the HDS reaction with three different feeds: DMDS, DBT and

industrial naphtha and results are shown in Fig. 9. Co-Mo/HAP-C nano-catalyst was tested with DMDS feed which showed higher conversion than other two feed stocks.

Since DBT is an aromatic compound, and removal of sulfur from DBT is more difficult than other feed stocks, and also the conversion for HDS reaction of industrial naphtha and DMDS are similar, thus one might conclude that the most of sulfur compounds of naphtha are linear like DMDS. Generally linear compounds like DMDS are more reactive than aromatic compounds that are in agreement with our results.

3.4. Reaction Kinetics

The equation used to calculate the rate constant for conversion of feed's sulfur into non harmful sulfur product, for first order reactions, is shown below [34]:

k_{HDS} = (LHSV) ln (S_f/S_p)

Where k_{HDS} is rate constant, S_p is the sulfur concentration in product, S_f is the concentration of sulfur in the feed and LHSV is the liquid hourly space velocity of feed. Single sulfur-containing compounds are generally known to obey first-order reaction kinetics [35, 36]. The HDS rate of DBT obeys pseudo-first-order reaction [38] and the naphtha HDS reaction, are generally represented by simple first-order kinetics [24].

In this study, the Co-Mo/HAP-C catalyst was tested in the HDS reaction with three different feed stocks. The rate constant of these reactions was calculated and results are shown in Table 3. According to these results DMDS feed showed very high activity, almost three times higher than those observed for the DBT feed. The rate constant of industrial naphtha feed is near DMDS rate constant. Elimination of sulfur from aromatic compounds is more difficult than linear compounds so rate constant for HDS reaction of DBT is lower than rate constant of DMDS HDS reaction.

The HDS rate constant of DMDS over Co-Mo/HAP catalyst versus time of reaction is presented in Table 4 and compared with that over the reference commercial catalyst (Co-Mo/Al_2O_3). It can be seen that as the time was increased, the overall HDS rate constant directly increased. For investigating the effect of time, samples were collected after each 2 h and its total sulfur were determined. For Co-Mo/HAP catalyst rate constant after 24 h was 19.49 h^{-1} while for commercial catalyst (Co-Mo/Al_2O_3) was 4.46 1/h. In other words, at the

same condition the rate constant for HDS reaction of DMDS over Co-Mo/HAP catalyst is higher than that of the commercial catalyst.

3.5. Effect of the acid-base properties of the support

It is known for many years that the nature and especially acid-base properties of the support can have a substantial effect on the catalytic properties of MoS_2 [38]. The acid-base properties of the support can also affect the dispersion as well as the geometric and electronic properties of the active component.

It is shown that acidic supports such as zeolites can promote the hydrogenation activity of the sulfides. However, in this study we have focused on the studies related to the HDS reaction. Muralidhar and his coworkers [39] studied the HDS of thiophene over various supported Co-Mo catalysts. They compared Co-Mo/Al_2O_3 to Co-Mo supported on SiO_2-Al_2O_3, SiO_2-MgO and TiO_2. They realized that the Co-Mo/Al_2O_3 catalyst was more active than the others in HDS process, which they attributed to a better dispersion of the Mo phase on alumina. It should be mentioned that alumina supported catalyst was less active in hydrocracking of 2,4,4-trimethylpentene which was an indication that it was less acidic than the other catalysts. As a matter of fact, by increasing the SiO_2 content in the SiO_2-Al_2O_3 mixed oxide, the HDS activity decreases, and the hydrocracking activity increases. It is clear that by increasing the SiO_2 content of the SiO_2-Al_2O_3 mixed oxide, its acidity increases [40], and its effect on hydrocracking was indeed expected.

Among the various supports which were used in this context, MgO and other materials containing MgO or other basic compounds received particular attention. Many patents recommended the use of MgO supported catalysts for selective HDS of FCC gasoline [38,40]. The gain in HDS activity resulting from increasing the basicity of the support was attributed to the fact that the size of the MoS_2 crystallites increased with enhancing the basicity as compared to their size on alumina. When we talk about increasing the size of the MoS_2 crystallites, it also shows itself in the thickness as well. This means that if the HDS reaction occurs at edge sites, then by increasing the basicity of the support, the proportion of edge versus corner sites increases.

Temperature program CO_2 desorption experiments (Fig. 7) showed that Co-Mo/HAP and Co-Mo/HAP-C after reduction have similar basicity, but Co-Mo/HAP-C is less active than Co-Mo/HAP which has a much lower surface area. We think the presence of carbon in

this catalyst not only has changed the morphology of the catalyst, but also it became more hydrophobic and then one might expect that the salts on the surface have more tendencies for aggregation. Catalytic activities of Co-Mo/HAP, Co-Mo /HAP-C and some previously reported catalysts in HDS reaction are shown in Table 5.

4. Conclusions

Hydroxyapetite-supported Co-Mo hydrodesulphurization catalysts were synthesized by loading cobalt and molybdenum onto calcined and pyrolyzed bone to give the Co-Mo/HAP and Co-Mo/HAP-C catalysts (molar ration of the Co:Mo was 0.33). In an attempt to prepare a Co-Mo/HAP by osmosic method we were not successful because the diffusion of cobalt into the bone framework did happen more efficiently than molybdenum, and the molar ratio of the loaded Co:Mo was 1.84. As the supports for HDS catalysts, the calcined and pyrolyzed bone because of different surface areas provided different size of nanoparticles of sulfide CoMo clusters. The hydrodesulphurization activity of these new catalysts was much higher than that of their alumina supported counterpart.

5. Acknowledgements

Thanks are due to Research Council of Isfahan University of Technology and the Center of Excellence in the Chemistry Department of Isfahan University of Technology and Research Institute of Petroleum Industry for supporting this work.

Notes and References:

[1] S. Brunet, D. Mey, J. Perot, C. Bouchy, F. Diehl, *Appl. Catal. A: Gen.,* 2005, **278**, 143.

[2] B. Hinnemann, P.G. Moses, J.K. Norskov, *J. Phys: Condens. Matter*., 2008, **20**, 064236 (8PP).

[3] E. R. Castellon, A.J. Lopez, D.E. Quesada, *Fuel*, 2008, **87**, 1195.

[4] H. Wang, E. Iglesia, *ChemCatChem*., 2011, **3**, 1166.

[5] H. Farag, D.D. Whitehurst, K. Sakanishi, I. Mochida, *Catal. Today*, 1999, **50**, 9.

[6] Y. Okamoto, *Catal. Today*, 2008, **132**, 9.

[7] R. Palcheva, L. Kaluza, A. Spojakina, K. Jiratova, G. Tyuliev, *Chin. J. Catal*., 2012, **33**, 952.

[8] K.V.R. Chary, H. Ramkrishna, K.S. Rama Rao, G. MuraliDhar, P. KantaRao, *Catal. Lett*., 1991, **10**, 27.

[9] K.C. Pratt, J.V. Sanders, V. Chritov, *J. Catal*., 1990, **124,** 416.

[10] G. Li, W. Li, M. Zhang, K. Tao, *Appl. Catal. A: Gen*., 2004, **273**, 233.

[11] P. Schacht, G. Hernandez, L. Cedeno, J. H. Mendoza, S. Ramirez, L. Garcia, J. Ancheyta, *Energy Fuels*. 2003, **17**, 81.

[12] Z.B. Wei, W. Yan, H. Zhang, T. Ren, Q. Xin, Z. Li, *Appl. Catal. A: Gen*., 1998, **167**, 39.

[13] H. Chen, X. Zhou, H. Shang, C. Liu, G. Qiu, F. Wei, *J. Nat. Gas Chem*. 2004, **13**, 209.

[14] J.L. Brito, F. Severino, N. Ninoska Delgado, J. Laine, *Appl. Catal. A: Gen*., 1998, **173**, 193.

[15] L. Kaluza, M. Zdrazil, *Carbon*. 2001, **39**, 2023.

[16] B. W. De Bonta, M. J. Vissenberg, V.H. J. De Beer, J.A.R. Van Veen, R.A. Van Santen, *Appl. Catal. A: Gen*., 2000, **202**, 99.

[17] P. Kovacheva, N. Davidova, J. Novakova, *Zeolites*, 1991, **11**, 54.

[18] A. Wang, Y. Wang, T. Kabe, Y. Chen, A. Ishihara, W. Qian, *J. Catal*. 2001, **199**, 19.

[19] B. Pawelec, S. Damyanova, R. Mariscal, J.L.G. Fierro, I. Sobrados, J. Sanz, L. Petrov, *J. Catal*. 2004, **223**, 86.

[20] T. Chiranjeevi, P. Kumar, M.S. Rana, G. MuraliDhar, T.S.R. PrasadaRao, *J. Mol. Catal. A: Chem*., 2002, **181**, 109.

[21] C. Rey, C. Combes, C. Drouet, M. J. Glimcher, *Osteoporos Int*., 2009, **20**, 1013.

[22] A. Mardani Ghahfarrokhi, P. Moshiri, M. Ghiaci, *Appl. Catal. A*: *Gen.*, 2013, **456**, 51.

[23] B. H. Monjezi, M. E. Yazdani, M. Mokfi, M. Ghiaci, *J. of Mol. Catal. A: Chem.,* 2014, **383-384**, 58.

[24] G. J. Fintos, F. M.Fiitani (Eds.), *Catalytic Naphtha Reforming*, Marcel Dekker, Inc. New York, 2004.

[25] H. Wang, R. Prins, *J. Catal*. 2009, **264**, 31.

[26] J. Ramirez, R. Contreras, P. Castillo, T. Klimova, *Appl. Catal. A: Gen*., 2000, **197**, 69.

[27] F. Liu, S. Xu, Y. Chi, D. Xue, *Catal. Commun*. 2011, **12**, 521.

[28] J.B. Condon, Surface Area and Porosity Determinations by Physisorption Measurements and Theory, Elsevier, Amsterdam, 2006.

[29] Z. Yu, L. Fareid, K. Moljord, E. A. Blekkan, J. C. Walmsley, D. Chen, *Appl. Catal. B: Environ.*, 2008, **84**, 482.

[30] H. Ge, X. Li,Z. Qin, F. Liang, J. Wang, *Korean J. Chem. Eng*., 2009, **26**, 576.

[31] H. Hattori, *Appl. Catal. A: Gen*., 2001, **222**, 247.

[32] R. Zavoianu, O. D. Pavel, A. Cruceanu, C. Preda, C. S. Nitu, E. Angelescu, *Prog. Catal*., 2003, **12**, 83.

[33] C. H. Bartholomew, P. K. Agrawal, J. R. Katzer, *Adv. Catal*., 1982, **31**, 135.

[34] M. Hqj, K. Linde, T. Klint Hansen, M. Brorson, A. Degn Jensen, *Appl. Catal. A: Gen*., 2011, **397**, 201.

[35] P. Robinson, E. Dolbear, *hydrotreating and hydrocracking: Fundamentals, in Practical Advances in Petroleum Processing*, Springer, 2006, pp 177-218.

[36] S. T. Sie, *Fuel Process. Technol*., 1999, **61**, 149.

[37] U. Riaz,O. J. Cumow, M. David Curtis, *J. Am. Chem. Soc*., 1994, **116**, 4357.

[38] P. Steiner, E. Blekkan, *Fuel Process. Technol*., 2002, **79**, 1.

[39] M. Breysse, J.L. Portefaix, M. Vrinat, *Catal. Today* 1991, **10**, 489.

[40] G. Muralidhar, F.E. Massoth, J. Shabtaı, *J. of Catal*., 1984, **85**, 44.

[41] K. Tanabe, *Solid Acids and Bases and their Catalytic Properties*, Academic Press, New York, 1970.

[42] J. P. R. Vissers, F. P. M. Mercx, *J. of Catal*., 1988, **114**, 291.

[43] M. A. Al-Daous, S. A. Ali, *Fuel,* 2012, **97**, 662.

[44] Y. Muhammad, C. Li, *Fuel Process. Technol*., 2011, **92**, 624.

Figure Captions

Fig. 1. IR spectra of a) HAP, b) HAP-C, c) Co-Mo/HAP, d) Co-Mo/HAP-C.

Fig. 2. DR-UV-Vis of a) HAP, b) HAP-C, c) Co-Mo/HAP, d) Co-Mo/HAP-C.

Fig. 3. The XRD patterns of (a) Co-Mo/HAP, (b) Co-Mo/HAP-C.

Fig. 4. Nitrogen adsorption-desorption isotherms of (a) Co-Mo/HAP and (b) Co-Mo/HAP-C catalysts.

Fig. 5. TEM micrographs of (a) Co-Mo/HAP-C, (b) Co-Mo/HAP.

Fig. 6. FE-SEM micrographs, and EDX spectra of (a) Co-Mo/HAP-C, and (b) Co-Mo/HAP.

Fig. 7(a). H_2–TPR profiles of a) HAP, b) Co-HAP, c) Mo-HAP

Fig. 7(b). H_2–TPR profiles of a) CoMo-HAP and b) CoMo-HAP-C catalysts.

Fig. 8. The CO_2-TPD spectra of (a) Co-Mo/HAP before reduction, (b) Co-Mo/HAP-C before reduction, (c) Co-Mo/HAP after reduction, (d) Co-Mo/HAP-C after reduction.

Fig. 9. Results of the HDS reaction with three different feed stocks over Co-Mo/HAP-C catalyst.

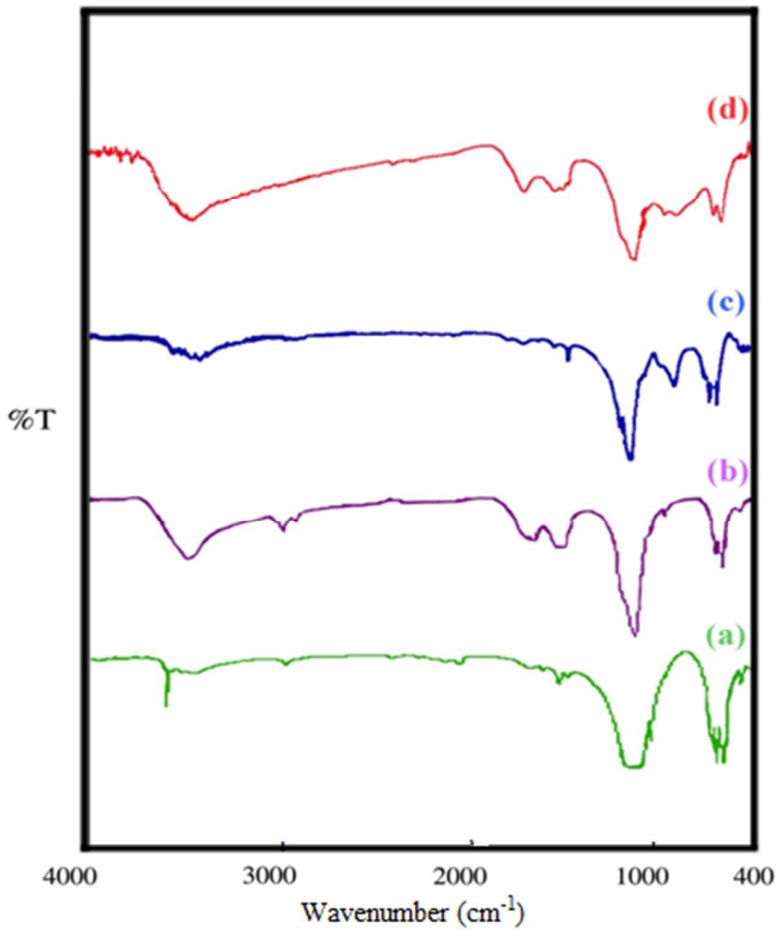

Fig. 1.

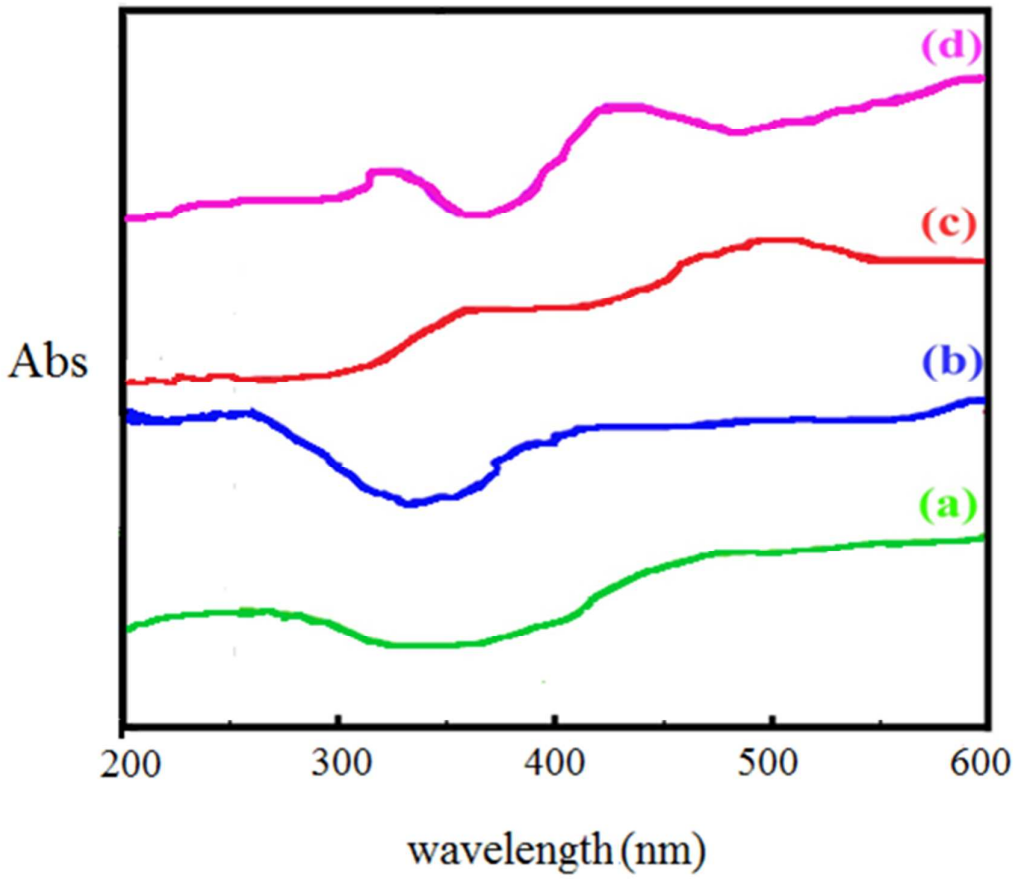

Fig. 2.

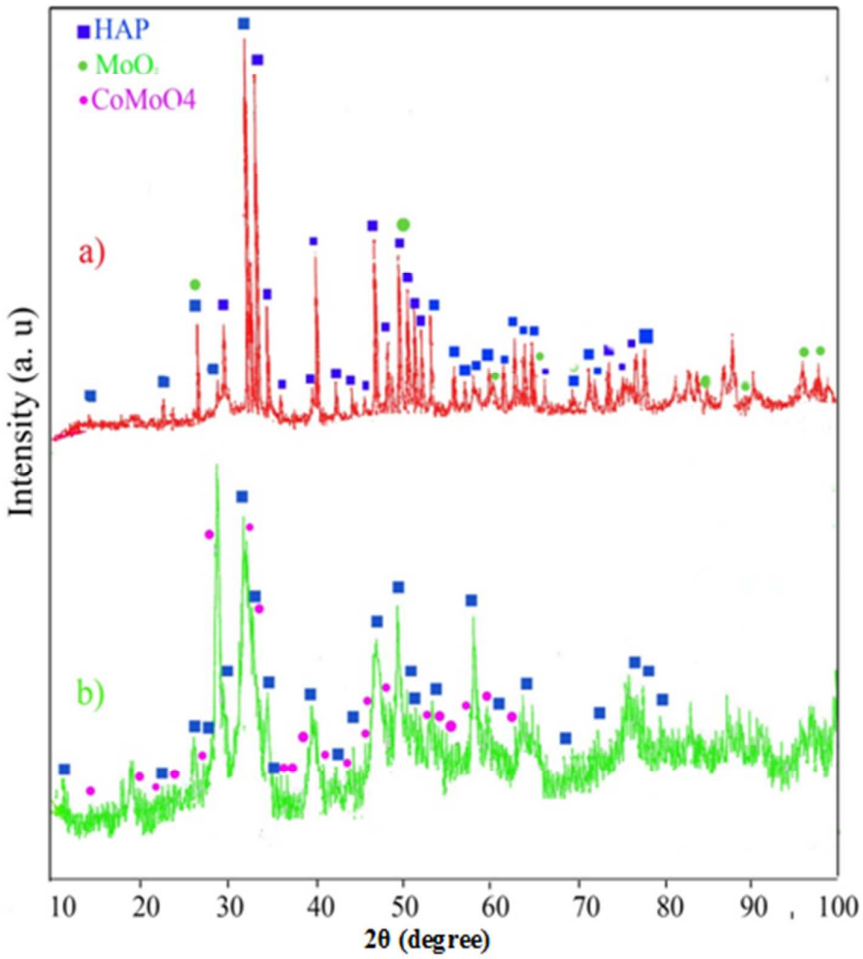

Fig. 3.

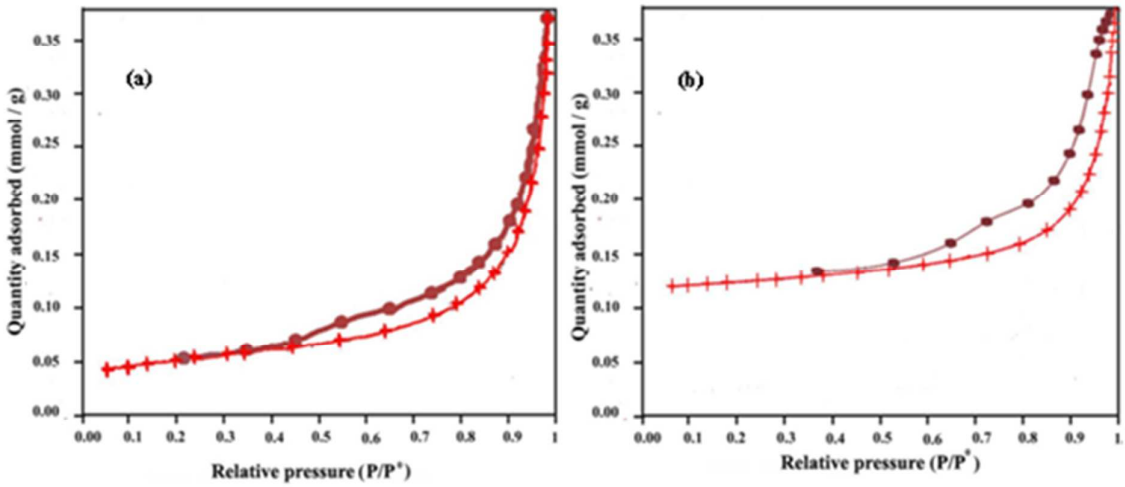

Fig. 4.

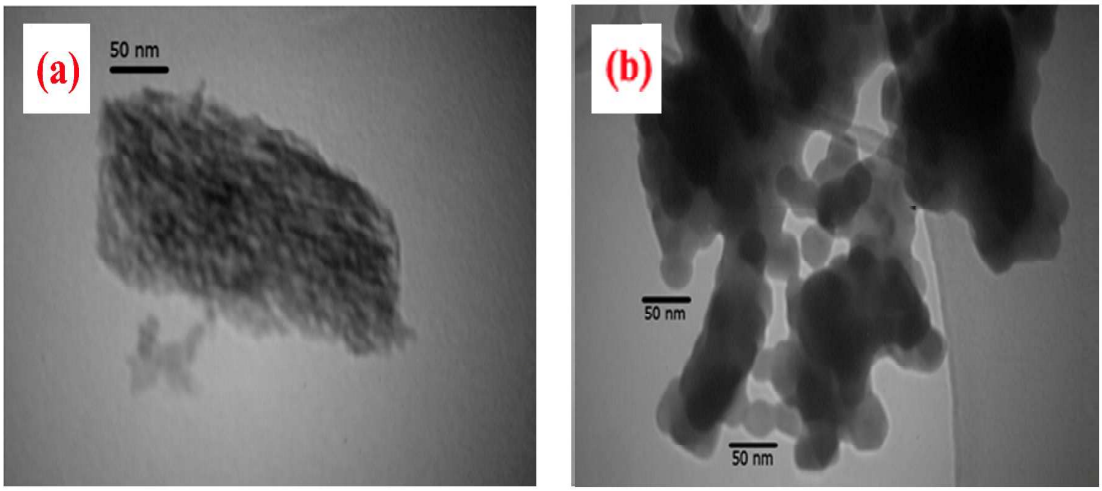

Fig. 5.

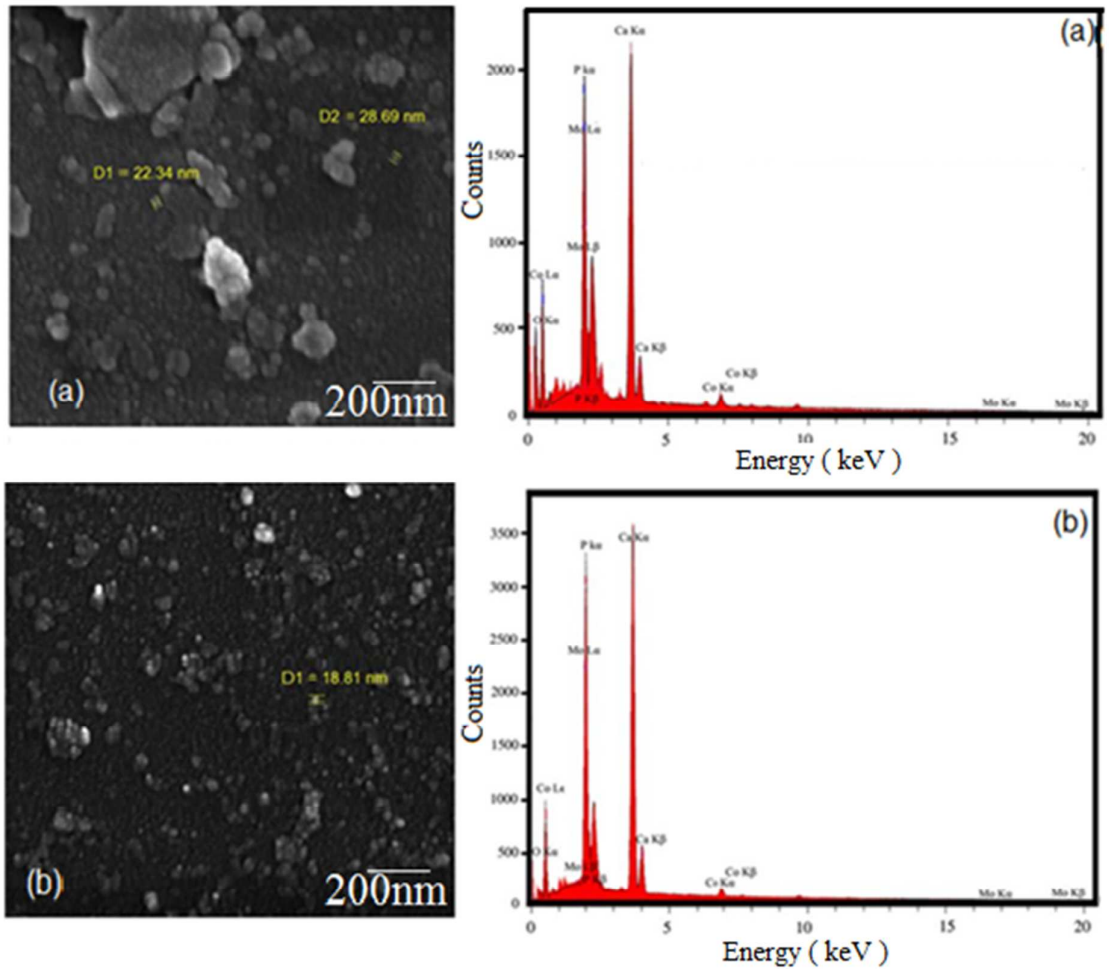

Fig. 6.

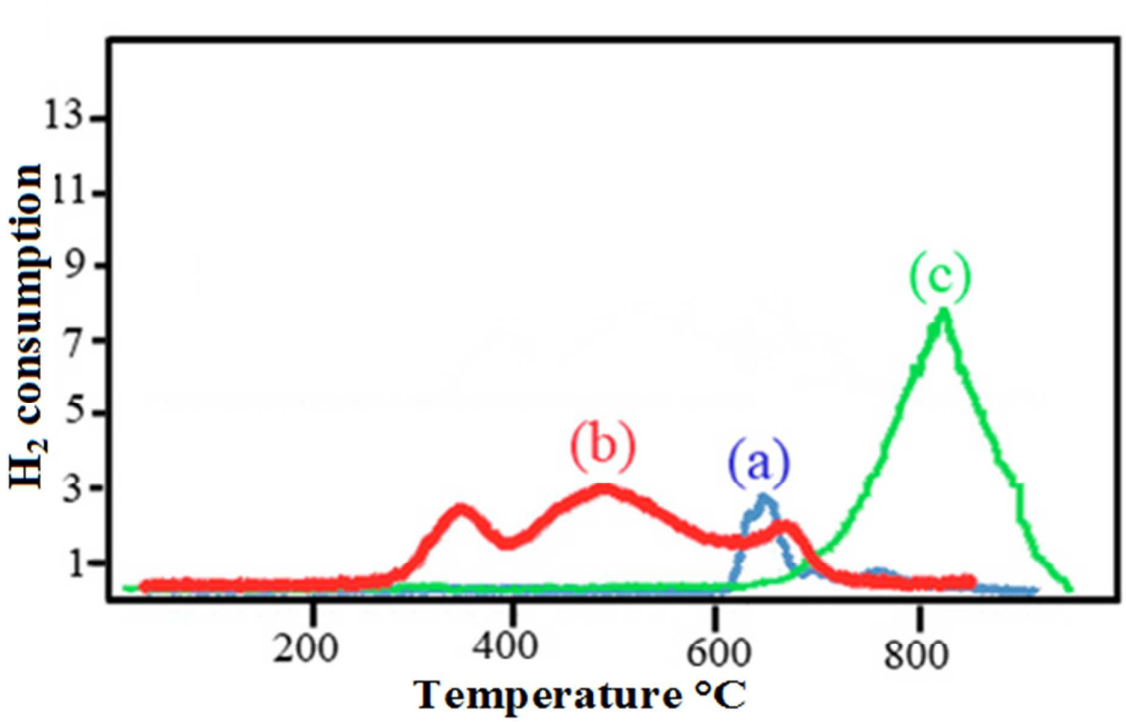

Fig. 7(a).

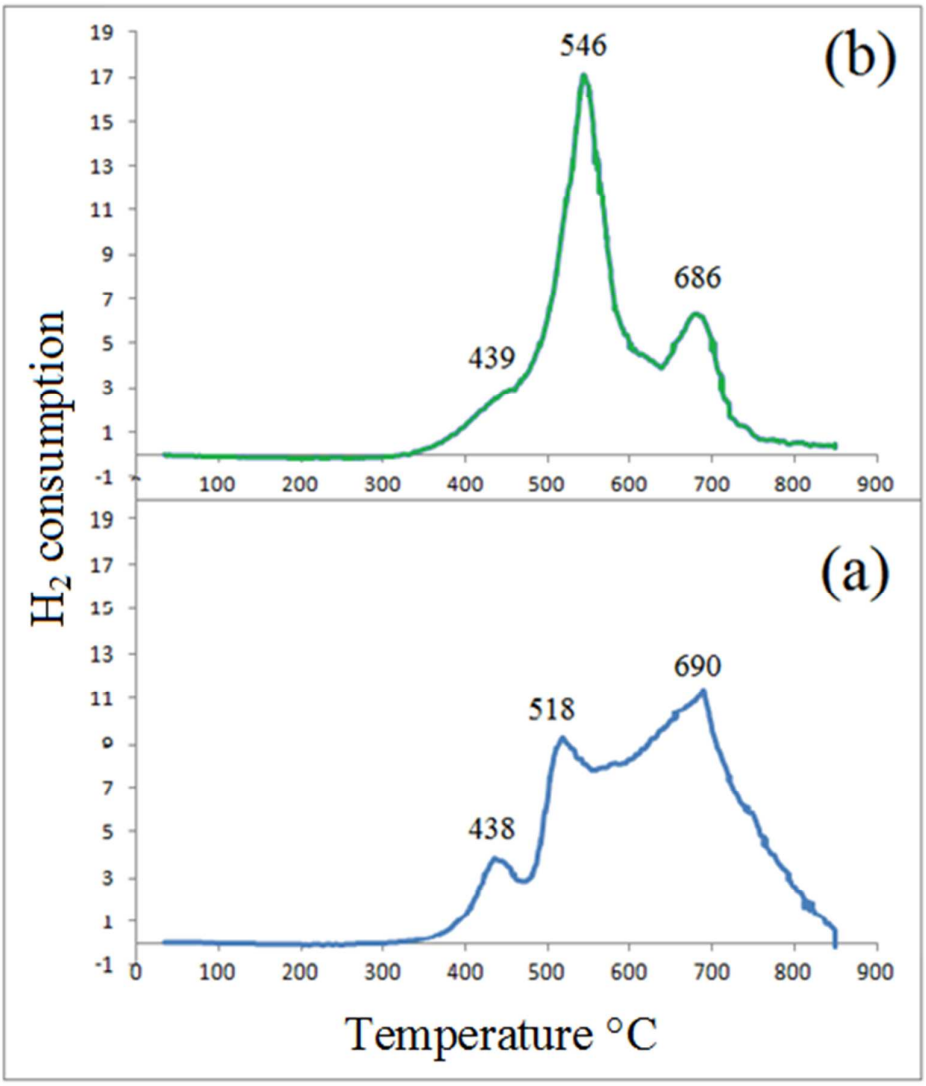

Fig. 7(b).

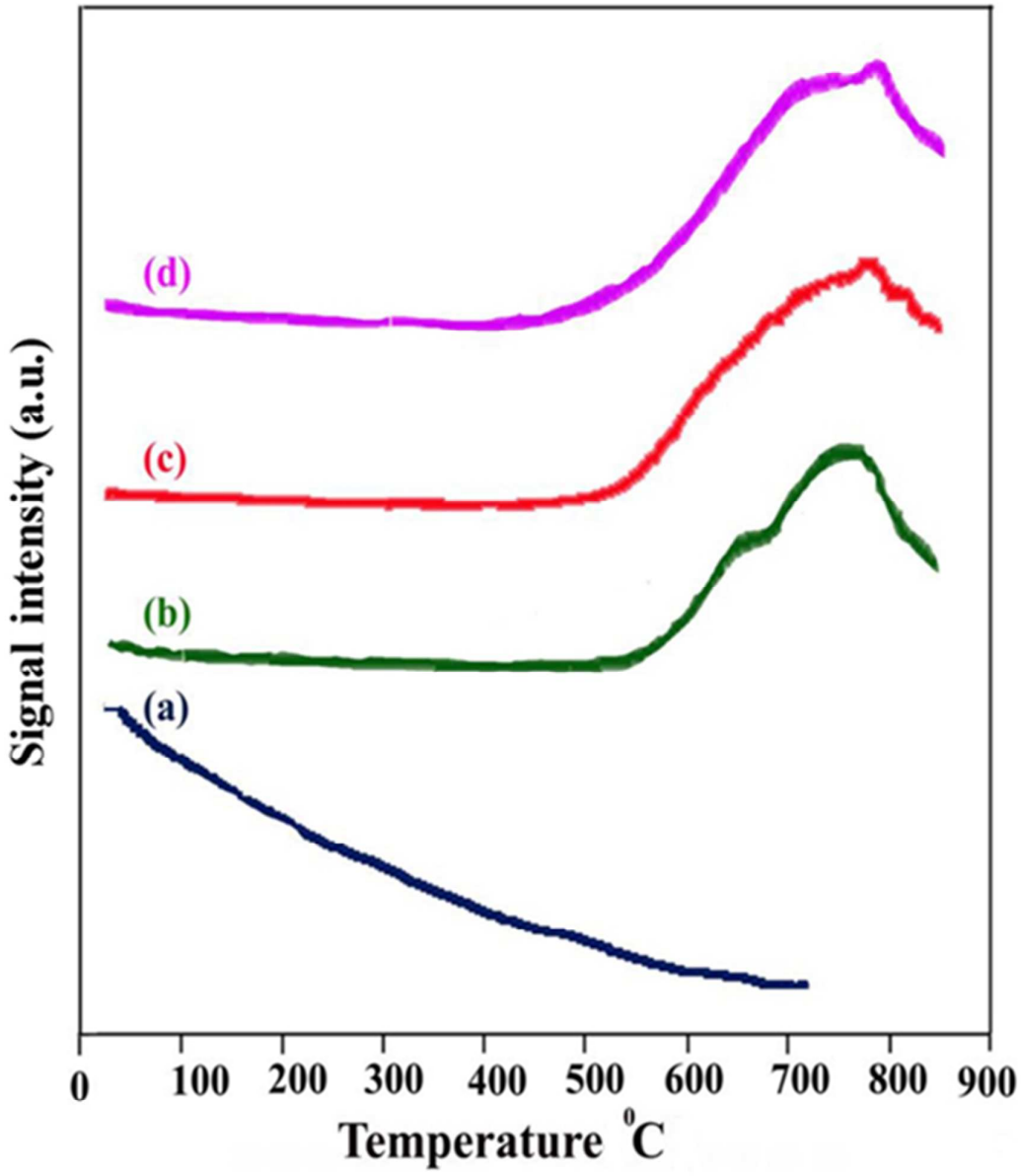

Fig. 8.

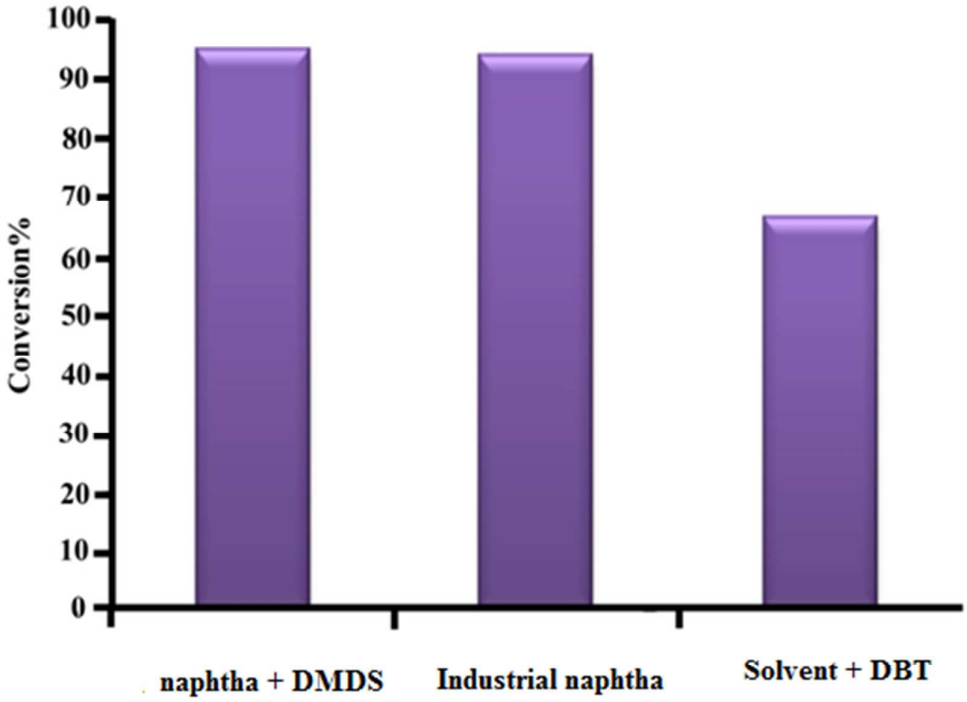

Fig. 9.

Table Captions

Table 1. Results of t-Plot, BET and Langmuir analysis.

Table 2. Residual sulfur content of naphtha after the HDS reaction.

Table 3. Rate constants of the HDS reactions of different feedstosks over Co-Mo /HAP-C. catalyst after 20 h

Table 4. Rate constants for the HDS reaction of dimethyl disulfide over different catalysts.

Table 5. Catalytic activities of Co-Mo/HAP, Co-Mo /HAP-C and some previously reported catalysts in HDS reaction.

Table 1. Results of t-Plot, BET and Langmuir analysis.

Catalyst	Co-Mo/HAP	Co-Mo/HAP-C
Micropore area (m^2/g)	1.44	28.87
External surface area (m^2/g)	2.75	72.83
Micropore volume (cm^3/g)	0.0007	0.0129
BET surface area (m^2/g)	4.19	101.70
Langmuir surface area (m^2/g)	5.65	137.99

Table 2. Residual sulfur content of naphtha after HDS reaction.

catalyst	Residual sulfur content of feed (ppm)	Time (h)
Co-Mo/HAP	33	20
Co-Mo/HAP	9	48
Co-Mo/HAP-C	110	20
Co-Mo/Al_2O_3	930	24
Co-Mo/Al_2O_3	107	48
Co-Mo/Al_2O_3	24	72

Reaction conditions: T = 310 ºC; P_{H2} = 15 bar; LHSV = 4.5 1/h; Feed contains 2510 ppm sulfur as DMDS.

Table 3.
Rate constants of the HDS reactions of different feedstosks over Co-Mo/HAP-C catalyst after 20 h.

Feed stock	Inatial sulfur content (ppm)	Residual sulfur content (ppm)	Rate constant
Industrial naphtha	2890	162	12.9
DMDS	2510	110	14.07
DBT	3370	1130	4.9

Reaction conditions: T = 310 ºC; P_{H2} = 15 bar; LHSV = 4.5 1/h; Co-Mo/ HAP-C catalyst; time = 20 h.

Table 4.

Rate constants for the HDS reactions of DMDS over different catalysts.

catalyst	Rate constant	Time of reaction (h)
Co-Mo/ HAP	19.49	24
Co-Mo/ HAP	25.33	48
Co-Mo/ Al_2O_3	4.46	24
Co-Mo/ Al_2O_3	14.19	48
Co-Mo/ Al_2O_3	20.09	72

Reaction conditions: T = 310 ºC; P_{H2} = 15 bar; LHSV = 4.5 1/h

Table 5. Catalytic activities of Co-Mo/HAP, Co-Mo /HAP-C and some previously reported catalysts in HDS reaction

Entry	Catalyst	Feed	%Conversion	Reference
1	Co-Mo/HAP	dimethyldisulfide	99.6	This work
2	Co-Mo/HAP-C	dimethyldisulfide	95.61	This work
3	Co-Mo/Ce-TiO_2	DBT	59.89	11
4	Co-Mo/La-TiO_2	DBT	60.45	11
5	Ni-Mo/Ac	thiophene	50	14
6	Tungstophosphoric/HMS	DBT	47.2	19
7	Co-Mo/alumina-MCM-41	DBT	76.43	26
8	Ni-Mo/Al2O3	thiophene	26.5	29
9	Ni-Mo/Al2O3-ZrO3	dimethyldisulfide	82	43
10	Pd-Ni-Mo/Al2O3	DBT	97	44